

arXiv:2301.12085v2 [cs.SI] 10 Mar 2023

arXiv:2301.12085v2 [cs.SI] 10 Mar 2023

arXiv:2301.12085v2 [cs.SI] 10 Mar 2023

arXiv:2301.12085v2 [cs.SI] 10 Mar 2023

arXiv:2301.12085v2 [cs.SI] 10 Mar 2023

arXiv:2301.12085v2 [cs.SI] 10 Mar 2023

arXiv:2301.12085v2 [cs.SI] 10 Mar 2023

arXiv:2301.12085v2 [cs.SI] 10 Mar 2023

arXiv:2301.12085v2 [cs.SI] 10 Mar 2023



arXiv:2301.12085v2 [cs.SI] 10 Mar 2023

arXiv:2301.12085v2 [cs.SI] 10 Mar 2023

arXiv:2301.12085v2 [cs.SI] 10 Mar 2023

arXiv:2301.12085v2 [cs.SI] 10 Mar 2023

arXiv:2301.12085v2 [cs.SI] 10 Mar 2023

been deployed massively in multi-user mobile edge computing (MEC) networks to improve the communication resource, and quality of service [13]–[15]. For instance, [13] considered dynamic user pairing NOMA-based offloading and established an energy consumption minimization framework by joint optimizing pairing. There is few work incorporating FL into MAR, and we only found one paper [16]. An FL-based mobile edge computing paradigm was proposed in [16] to solve object recognition and classification problem without considering optimizing the resource allocation in the framework.

Novelty. The previously mentioned studies [13]–[15] were only about NOMA and MEC systems without integrating FL and MAR. [16] was about FL and AR without considering resource allocation. Additionally, although [7]–[12] were related to resource allocation and MAR, they did not apply FL to their systems. In this paper, we consider a basic FL-assisted MAR system via NOMA, and design an algorithm to jointly optimize time, energy and model accuracy simultaneously. Besides, we take into account the different requirements in diverse situations. For example, we prefer to optimize energy consumption as much as possible when the mobile device is low on power. So, the objective function includes a weighted combination of total energy consumption, completion time and model accuracy and allows the weights to be adjusted to achieve different optimization results.

Contributions. The contributions of our paper are as follows:

- To our best knowledge, we are the first to introduce FL assisted NOMA system in MAR to enhance the model performance, which could improve the experience of users in the Metaverse.
- An optimization algorithm is proposed to optimize time, energy, and accuracy jointly. The weights of them could be adjusted freely according to practical situations.
- Detailed comparative experiments, convergence analysis and time complexity, are provided to show the robustness and effectiveness of our method.

II. SYSTEM MODEL

We consider an MAR network with N cellular-connected MAR devices. All MAR devices transmit data to a BS through the uplink NOMA transmission protocol. Each device trains its own object detection model locally and collaboratively trains a global model through FL, as shown in Fig. 1. In this paper, bold symbols represent vectors. If a symbol x is a solution to a problem, then x^* means the optimal solution.

Uplink NOMA. In an uplink-NOMA system, through channel and power assignment, signals of devices are multiplexed on each channel. Assume there are N users and K channels. The higher the number of devices multiplexed on each channel, the higher the hardware complexity and latency. Thus, following [17], [18] and considering practicality, we suppose there are 2 users multiplexed on the k -th subchannel.

Suppose a user n belongs to the subchannel k , and it is the i -th ($i = 1, 2$) user in the subchannel k . Define $g_{k,i}$ as the channel gain between the base station and the i -th device on

channel k . Without loss of generality, assume $g_{k,i-1} < g_{k,i}$ on channel k and the information of the user with better channel gain will be decoded first by the base station.

User pairing. Similar to [14], we consider using the following user pairing schemes: (a) random selection: randomly selecting two users to form a group, (b) nearest-user-pairing: pairing two nearest users, then the next nearest users, and so forth, (c) nearest-farthest-pairing: the nearest user and the farthest user are formed into a group, then pairing the second nearest and the second farthest user, and so forth. In the resource allocation algorithm (Algorithm 2) stated in section III-E, three user pairing schemes are used, and the best one will be selected as the final result.

Federated learning. Assume there are D_n (i.e., $D_{k,i}$) samples on each device n (i.e., the i -th device on channel k). As shown in Fig. 1, each mobile device runs its own model locally and collaboratively solves the problem $\min_{\omega} F(\omega) = \sum_{n=1}^N \frac{D_n}{\sum_{n=1}^N D_n} l_n(\omega)$, where $l_n(\cdot)$ denotes the loss function per sample and ω is the global model. After each device finishes its local training for a certain number of iterations, it will upload the model parameter to the base station. Next, the base station will calculate the weighted average model parameter $\frac{\sum_{n=1}^N D_n \omega_n}{\sum_{n=1}^N D_n}$ and send it back to each device. Such uploading and broadcasting process is called one *global communication round*.

A. Energy and Time Consumption

We only study the process between two global communication rounds. We define the *total energy consumption* as \mathcal{E} , and it includes wireless *transmission energy* and *local computation energy*. The *total time consumption* is defined as \mathcal{T} . It consists of *transmission time* and *local computation time*. Following [19], [20], the energy consumed at the base station is not considered.

Transmission energy. In light of the fact that the base station's output power is significantly greater than the uplink transmission power of a mobile device, the downlink time is ignored in this work. Hence, according to the Shannon formula, the data transmission rate of the i -th user on channel k is

$$r_{k,i} = B_k \log_2 \left(1 + \frac{p_{k,i} g_{k,i}}{B_k N_k + \sum_{j=0}^{i-1} p_{k,j} g_{k,j}} \right), \quad (1)$$

and we define $p_{k,0} = 0$. We denote the total bandwidth is B , and $B_k = \frac{B}{K}$. $p_{k,i}$ refers to the transmission power. $g_{k,i}$ is the channel between the base station and the i -th device on channel k . N_k is the noise power spectral density of Gaussian noise. Suppose the transmission data size of each device is $d_{k,i}$, so the transmission time of the i -th user on channel k is

$$T_{k,i}^{\text{trans}} = d_{k,i} / r_{k,i}. \quad (2)$$

Therefore, the corresponding transmission energy is

$$E_{k,i}^{\text{trans}} = p_{k,i} T_{k,i}^{\text{trans}}. \quad (3)$$

Local computation energy. We incorporate You Only Look Once (YOLO) algorithm [21] to handle the object detection tasks on each device. Note that the main structure of YOLO is convolutional neural network (CNN). Assume on the i -th device on channel k , the video frame resolution used for training is $s_{k,i} \times s_{k,i}$ pixels. Thus, due to the influence of

the frame resolution used for training on computing resources [22] and motivated by [23], the local computation energy is defined as

$$E_{k,i}^{cmp} = \kappa \eta \xi s_{k,i}^2 c_{k,i} D_{k,i} f_{k,i}^2, \quad (4)$$

where κ represents the effective switched capacitance, η is the number of local iterations, $s_{k,i}^2$ is the pixels of the frame resolution, $D_{k,i}$ is the number of samples, $f_{k,i}$ is the CPU frequency and $c_{k,i}$ is the number of CPU cycles per *standard sample*. We define the *standard sample* as a video frame with a resolution of $s_0 \times s_0$ pixels and $\xi = \frac{1}{s_0^2}$. This means if a video frame with $s_{k,i}^2$ pixels and $s_{k,i} = s_0$, the local computation energy will be $\kappa \eta c_{k,i} D_{k,i} f_{k,i}^2$, which is the same as the definition in [23].

Hence, the total energy consumption \mathcal{E} is

$$\mathcal{E} = \sum_{k=1}^K \sum_{i=1}^2 (E_{k,i}^{trans} + E_{k,i}^{cmp}). \quad (5)$$

Transmission time. This is given in Eq. (2).

Computation time. The local computation time (i.e., the local training time) of the i -th device on channel k in one global iteration is

$$T_{k,i}^{cmp} = \eta \frac{\xi s_{k,i}^2 c_{k,i} D_{k,i}}{f_{k,i}}. \quad (6)$$

Thus, the total completion time is

$$\mathcal{T} = \max\{T_{k,i}^{trans} + T_{k,i}^{cmp}\}, \quad i = 1, 2, \quad k \in [1, K]. \quad (7)$$

B. Accuracy Analysis

Denote \mathcal{A} be the training accuracy of the whole federated learning process and define it as a function of $s_{k,i}$, which is $\mathcal{A}(s_{1,1}, s_{1,2}, \dots, s_{K,1}, s_{K,2}) = \sum_{k=1}^K \sum_{i=1}^2 \mathcal{A}_{k,i}$.

The accuracy model from [24] is used in this work. Based on YOLO algorithm, [24] constructs the accuracy function regarding different video frame resolutions. Thus, the accuracy function of the i -th user on channel k is defined as

$$\mathcal{A}_{k,i} = 1 - 1.578e^{-6.5 \times 10^{-3} s_{k,i}}. \quad (8)$$

III. JOINT OPTIMIZATION OF ENERGY, TIME AND ACCURACY WITH FIXED USERS

In this section, problem formulation, problem decomposition and solutions to the optimization problem will be illustrated, respectively.

A. Problem Formulation

A joint optimization of energy \mathcal{E} , time \mathcal{T} and accuracy \mathcal{A} problem is formulated in this section. The optimization problem is as follows:

$$\min_{s_{k,i}, f_{k,i}, p_{k,i}} \alpha \mathcal{E} + \beta \mathcal{T} - \gamma \mathcal{A}, \quad (9)$$

$$\text{subject to, } p^{min} \leq p_{k,i} \leq p^{max}, \quad k \in [1, K], \quad i = 1, 2, \quad (9a)$$

$$f^{min} \leq f_{k,i} \leq f^{max}, \quad k \in [1, K], \quad i = 1, 2, \quad (9b)$$

$$s_{k,i} \in \{s_1, s_2, s_3\}, \quad (9c)$$

where $s_{k,i}$, $f_{k,i}$ and $p_{k,i}$ are three optimization variables. α , β and γ are three weight parameters, and $\alpha + \beta = 1$, $\alpha, \beta \in [0, 1]$, and $\gamma \geq 0$. Constraints (9a) and (9b) limit the ranges of the transmission power and CPU frequency of each device. Constraint (9c) sets three choices for the video frame resolution and $s_1 < s_2 < s_3$.

Due to the max function of \mathcal{T} , problem (9) is non-convex and difficult to be decomposed. To avoid this difficulty, an

auxiliary variable T is introduced, and the problem becomes:

$$\min_{s_{k,i}, f_{k,i}, p_{k,i}, T} \alpha \left(\sum_{k=1}^K \sum_{i=1}^2 E_{k,i}^{cmp} + E_{k,i}^{trans} \right) + \beta T - \gamma \mathcal{A}, \quad (9)$$

subject to, (9a), (9b), (9c)

$$T_{k,i}^{trans} + T_{k,i}^{cmp} \leq T, \quad i \in \{1, 2\}, \quad k = 1, \dots, K, \quad (10a)$$

where constraint (10a) is considered an upper bound of the total time consumption.

B. Problem Decomposition

Due to the original optimization problem (9) being non-convex and quite complex, we split it into two subproblems (*SP1* and *SP2*) to make it easier to solve. Since $p_{k,i}$ only appears in $E_{k,i}^{trans}$, two subproblems are constructed, one with the optimization variable $f_{k,i}$ and $s_{k,i}$, and the other with $p_{k,i}$.

Subproblems 1 and 2 write as follows:

$$\textbf{SP1:} \quad \min_{s_{k,i}, f_{k,i}, T} \alpha \left(\sum_{k=1}^K \sum_{i=1}^2 E_{k,i}^{cmp} \right) + \beta T - \gamma \mathcal{A}, \quad (11)$$

subject to, (9b), (9c), (10a).

$$\textbf{SP2:} \quad \min_{p_{k,i}} \alpha \sum_{k=1}^K \sum_{i=1}^2 \frac{p_{k,i} d_{k,i}}{r_{k,i}}, \quad (12)$$

subject to, (9a), (10a).

C. Solution to SP1

Since the video frame resolution $s_{k,i}$ is discrete, we relax it into a continuous variable $\hat{s}_{k,i}$ to make *SP1* easier to tackle. Next, we handle $A_{k,i}(\hat{s}_{k,i})$. Because our research mainly focuses on the application of federated learning in NOMA, so we introduce a simple but effective linear approach to construct the function $A_{k,i}$ (8). By using two points $(s_1, A_{k,i}(s_1))$ and $(s_3, A_{k,i}(s_3))$, we approximate $A_{k,i}(\hat{s}_{k,i})$ as the following linear function $\hat{A}_{k,i}(\hat{s}_{k,i})$:

$$\hat{A}_{k,i}(\hat{s}_{k,i}) = \hat{k}_{k,i}(\hat{s}_{k,i} - s_1) + A_{k,i}(s_1), \quad (13)$$

where $\hat{k}_{k,i} = \frac{A_{k,i}(s_3) - A_{k,i}(s_1)}{s_3 - s_1}$.

Then, the *SP1* becomes:

$$\min_{s_{k,i}, f_{k,i}, T} \alpha \sum_{k=1}^K \sum_{i=1}^2 E_{k,i}^{cmp} + \beta T - \gamma \sum_{k=1}^K \sum_{i=1}^2 \hat{A}_{k,i}(\hat{s}_{k,i}) \quad (14)$$

subject to, (9b), (10a),

$$s_1 \leq \hat{s}_{k,i} \leq \hat{s}_3, \quad \forall k \in [1, K], \quad i = 1, 2. \quad (14a)$$

It is easy to verify that the function of *SP1* is convex, and the constraints are also. Karush-Kuhn-Tucker (KKT) approach works well to get the optimal solutions for this optimization problem.

After applying KKT conditions, we get

$$f_{k,i}^* = \sqrt[3]{\frac{\lambda_{k,i}}{2\alpha\kappa}}, \quad \hat{s}_{k,i}^* = \frac{\gamma \hat{k}_{k,i}}{2\eta \xi c_{k,i} D_{k,i} (\alpha \kappa f_{k,i}^2 + \frac{\lambda_{k,i}}{f_{k,i}})}, \quad (15)$$

$$\beta = \sum_{k=1}^K \sum_{i=1}^2 \lambda_{k,i}, \quad (16)$$

where $\lambda_{k,i}$ is the Lagrange multiplier associated with the inequality constraint (10a).

Through Eq. (15), we can use $\lambda_{k,i}$ to represent $f_{k,i}$ and $\hat{s}_{k,i}^2$. Then, we can get the dual problem as follows:

$$\max_{\lambda_{k,i}} \sum_{k=1}^K \sum_{i=1}^2 - \frac{\gamma^2 \hat{k}_{k,i}^2}{4h(2^{-\frac{2}{3}} + 2^{\frac{1}{3}})} \lambda_{k,i}^{-\frac{2}{3}} + T_{k,i}^{up} \lambda_{k,i} + \gamma \hat{k}_{k,i} s_1 - \gamma A_{k,i}(s_1) \quad (17)$$

subject to, (16), $\lambda_{k,i} \geq 0$,

where $h = \eta \xi_{C_{k,i}} D_{k,i} (\alpha \kappa)^{\frac{1}{3}}$. Obviously, this dual problem is a simple convex optimization problem. In this paper, we use CVX [25] to solve it and get the optimal $\lambda^* = [\lambda_{1,1}^*, \dots, \lambda_{K,2}^*]$. Then we can leverage the λ^* to calculate the optimal f^* and \hat{s}^* through Eq. (15). With the constraint of $f^{min} \leq f_{k,i} \leq f^{max}$, we can get $f_{k,i}^*$ in the below:

$$f_{k,i}^* = \min(f^{max}, \max(f_{k,i}^*, f^{min})). \quad (18)$$

Since the frame resolution $s_{k,i}$ is discrete, we adopt the following formula to map $\hat{s}_{k,i}$ to $s_{k,i}$:

$$s_{k,i}^* = \begin{cases} s_3, & \text{if } \hat{s}_{k,i} > \frac{s_2 + s_3}{2} \\ s_2, & \text{if } \frac{s_1 + s_2}{2} \leq \hat{s}_{k,i} \leq \frac{s_2 + s_3}{2} \\ s_1, & \text{if } \hat{s}_{k,i} < \frac{s_1 + s_2}{2} \end{cases} \quad (19)$$

$SP1$ is solved. Next, $SP2$ will be explained.

D. Solution to $SP2$

The objective function (12) of $SP2$ is non-convex, since it is easy to verify that its Hessian matrix is not positive semidefinite. On channel k , the forms of $r_{k,1}$ and $r_{k,2}$ are different. Hence, to continuously simplify $SP2$, we decompose it into another two subproblems— $SP2_1$ with optimization variable $p_{k,1}$ and $SP2_2$ with $p_{k,2}$.

$$SP2_1 : \min_{p_{k,1}} \alpha \left(\sum_{k=1}^K \frac{p_{k,1} d_{k,1}}{B_k \log_2(1 + \frac{p_{k,1} g_{k,1}}{B_k N_k})} \right), \quad (20)$$

$$\text{subject to, (9a), } r_{k,1} \geq r_{k,1}^{min}, \quad (20a)$$

$$SP2_2 : \min_{p_{k,2}} \alpha \left(\sum_{k=1}^K \frac{p_{k,2} d_{k,2}}{B_k \log_2(1 + \frac{p_{k,2} g_{k,2}}{B_k N_k + p_{k,1} g_{k,1}})} \right), \quad (21)$$

$$\text{subject to, (9a), } r_{k,2} \geq r_{k,2}^{min}, \quad (21a)$$

$$\text{where } r_{k,1}^{min} = \frac{d_{k,1}}{T - \frac{\eta c_{k,1} D_{k,1}}{f_{k,1}}}, \text{ and } r_{k,2}^{min} = \frac{d_{k,2}}{T - \frac{\eta c_{k,2} D_{k,2}}{f_{k,2}}}.$$

In fact, $SP2_1$ and $SP2_2$ are two minimization sum-of-ratios problems, which are NP-complete [26] and challenging to solve. Therefore, to further make them solvable, we transform $SP2_1$ and $SP2_2$ into the epigraph form. To be concise and due to the same property of $SP2_1$ and $SP2_2$, we write a general form as follows. Besides, for $SP2_1$, $\hat{p}_k = p_{k,1}$; for $SP2_2$, $\hat{p}_k = p_{k,2}$.

$$SP2_epi : \min_{\hat{p}_k, \Gamma_k} \alpha \sum_{k=1}^K \Gamma_k, \quad (22)$$

subject to, (9a), Constraint_1 ,

where Γ_k is the auxiliary variable and the constraint

$$\text{Constraint}_1 = \begin{cases} SP2_1 : (20a), \frac{p_{k,1} d_{k,1}}{\hat{r}_k} \leq \Gamma_k, \\ \hat{r}_k = B_k \log_2(1 + \frac{p_{k,1} g_{k,1}}{B_k N_k}), \\ SP2_2 : (21a), \frac{p_{k,2} d_{k,2}}{\hat{r}_k} \leq \Gamma_k, \\ \hat{r}_k = B_k \log_2(1 + \frac{p_{k,2} g_{k,2}}{B_k N_k + p_{k,1} g_{k,1}}). \end{cases} \quad (23)$$

However, the above form is still non-convex. In $SP2_1$, since the only variable is $p_{k,1}$, it is obvious that $p_{k,1} d_{k,1}$ is convex, and $B_k \log_2(1 + \frac{p_{k,1} g_{k,1}}{B_k N_k})$ is concave. This means each term of the objective function has the characteristics—the numerator is convex and the denominator is concave. In addition, $SP2_2$ has the same characteristics. Because of such characteristics, we provide the following lemma to transform the subproblems into subtractive-form problems, which are equivalent to the original subproblems.

Lemma 1. *If $(\hat{p}_k^*, \Gamma_k^*)$ is the solution of $SP2_epi$, the following problem has \hat{p}_k^* as its solution if there exist $\nu_k = \nu_k^*$, $\Gamma_k = \Gamma_k^*$, $k = 1, \dots, K$.*

$$SP2_sub : \min_{\hat{p}_k} \sum_{k=1}^K \nu_k [\hat{p}_k \hat{d}_k - \Gamma_k \hat{r}_k], \quad (24)$$

subject to : (9a), Constraint_2 ,

where

$$\text{Constraint}_2 = \begin{cases} SP2_1 : (20a), \\ SP2_2 : (21a). \end{cases}$$

For $SP2_1$, $\hat{p}_k \hat{d}_k = p_{k,1} d_{k,1}$; for $SP2_2$, $\hat{p}_k \hat{d}_k = p_{k,2} d_{k,2}$.

Additionally, with $\nu_k = \nu_k^*$, $\Gamma_k = \Gamma_k^*$ and $\hat{p}_k = \hat{p}_k^*$, the following equations are satisfied:

$$\nu_k^* = \frac{\alpha}{\hat{r}_k}, \quad \Gamma_k^* = \frac{\hat{p}_k^* \hat{d}_k}{\hat{r}_k}, \quad k = 1, \dots, K. \quad (25)$$

proof. The proof is provided by Lemma 2.1 in [27].

In brief, Lemma 1 proves that $SP2_epi$ and $SP2_sub$ are equivalent and have the same optimal solution. Hence, both subproblems $SP2_1$ and $SP2_2$ can be transformed into the form of $SP2_sub$.

Thus, to solve $SP2_epi$, we can solve $SP2_sub$ to obtain \hat{p}_k with given ν_k and Γ_k . Next, with the obtained \hat{p}_k , we can calculate the new ν_k and Γ_k through Eq. (25).

To solve $SP2_sub$, applying KKT conditions, we can get

$$\hat{p}_k^* = \begin{cases} \frac{(\nu_k \gamma + \mu_k) B_k}{\nu_k d_{k,1} \ln 2} - \Lambda, & \mu_k = 0 \\ (2^{\frac{\hat{r}_k^{min}}{B_k}} - 1) \Lambda, & \mu_k > 0, \end{cases} \quad (26)$$

where $\mu_k = [2^{\frac{\hat{r}_k^{min}}{B_k}} \Lambda (\ln 2) \nu_k \hat{d}_k / B_k - \nu_k \Gamma_k]^+$ and $[x]^+$ means $\max(0, x)$. In addition,

$$\begin{cases} SP2_1 : \hat{p}_k = p_{k,1}, \hat{r}_k^{min} = r_{k,1}^{min}, \Lambda = \frac{B_k N_k}{g_{k,1}}, \\ SP2_2 : \hat{p}_k = p_{k,2}, \hat{r}_k^{min} = r_{k,2}^{min}, \Lambda = \frac{B_k N_k + p_{k,1} g_{k,1}}{g_{k,2}}. \end{cases} \quad (27)$$

We have finished converting $SP1$ and $SP2$. The algorithm for optimizing $SP2$ is listed in Algorithm 1. The original algorithm is given in [27] and is a Newton-like method.

In Algorithm 1, we define $\varphi(\Gamma_k, \nu_k) = [\varphi_1^T(\Gamma_k), \varphi_2^T(\nu_k)]^T$, where

$$\varphi_1(\Gamma_k) = [-\hat{p}_k \hat{d}_k + \Gamma_k \hat{r}_k]^T, \quad \varphi_2(\nu_k) = [-\alpha + \nu_k \hat{r}_k]^T, \quad k \in [1, K]. \quad (28)$$

The Jacobian matrices of $\varphi_1(\Gamma_k)$ and $\varphi_2(\nu_k)$ are

$$\varphi'_1(\Gamma_k) = \text{diag}(\hat{r}_k), \varphi'_2(\nu_k) = \text{diag}(\hat{r}_k), k \in [1, K], \quad (29)$$

where $\text{diag}()$ stands for a diagonal matrix.

Algorithm 1: Optimization of SP2_I/SP2_2

```

1 Initialize  $j = 0, \zeta \in (0, 1), \epsilon \in (0, 1)$  and feasible  $\hat{p}_k^0$ .
2 repeat
3   Calculate  $(\nu_k^{(j)}, \Gamma_k^{(j)})$  according to Eq. (25).
4   Get  $(\hat{p}_k^{(j+1)})$  by calculating Eq. (26).
5   Let  $i$  be the smallest integer satisfying
      
$$|\varphi(\Gamma_k + \zeta^i \sigma_{k,1}^{(j)}, \nu_k + \zeta^i \sigma_{k,2}^{(j)})|$$

      
$$\leq (1 - \epsilon \zeta^i) |\varphi(\Gamma_k^{(j)}, \nu_k^{(j)})|, \quad (30)$$

      where
      
$$\sigma_{k,1}^{(j)} = -[\varphi'_1(\Gamma_k^{(j)})]^{-1} \varphi_1(\Gamma_k^{(j)}),$$

      
$$\sigma_{k,2}^{(j)} = -[\varphi'_2(\nu_k^{(j)})]^{-1} \varphi_2(\nu_k^{(j)}), \quad (31)$$

6   Update
      
$$(\Gamma_k^{(j+1)}, \nu_k^{(j+1)}) = (\Gamma_k^{(j)} + \zeta^i \sigma_{k,1}^{(j)}, \nu_k + \zeta^i \sigma_{k,2}^{(j)}). \quad (32)$$

7    $j \leftarrow j + 1$ .
8 until  $\varphi(\Gamma_k, \nu_k) = \mathbf{0}$  or reaching the maximum
   iteration number  $J$ ;
```

E. Resource Allocation Algorithm

Based on Eq. (26), a resource allocation algorithm is proposed, which is an iterative optimization algorithm, as shown in Algorithm 2. It first initially assigns a feasible solution set within the range of \mathbf{f} , \mathbf{p} and \mathbf{s} . Next, iteratively solving SP1 (problem (17)) and SP2 (SP2_I & SP2_2) to obtain (\mathbf{f}, \mathbf{s}) and \mathbf{p} respectively until convergence.

Algorithm 2: Resource Allocation Algorithm

```

1 Initialize  $\mathbf{S}^{(0)} \leftarrow (\mathbf{f}^{(0)}, \mathbf{s}^{(0)}, \mathbf{p}^{(0)})$  of problem (9).
   Iteration number  $i = 1$ , the maximum number of
   iterations  $\mathcal{M}$ .
2 while  $|\mathbf{S}^{(i)} - \mathbf{S}^{(i-1)}| > \epsilon$  and  $i \leq \mathcal{M}$  do
3   Solve problem (17), which is the dual problem of
     SP1, to obtain  $(\mathbf{f}^{(i)}, \mathbf{s}^{(i)})$  through CVX given
      $\mathbf{p}^{(i-1)}$ .
4   Given  $(\mathbf{f}^{(i)}, \mathbf{s}^{(i)})$ , call Algorithm 1 ( $\hat{p}_k = p_{k,1}$ ) to
     solve SP2_I and get  $p_{k,1}^{(i)}$ .
5   Given  $p_{k,1}^{(i)}$ , call Algorithm 1 ( $\hat{p}_k = p_{k,2}$ ) to solve
     SP2_2 to obtain  $p_{k,2}^{(i)}$ .
6    $\mathbf{p}^{(i)} \leftarrow [p_{1,1}^{(i)}, \dots, p_{K,1}^{(i)}, p_{1,2}^{(i)}, \dots, p_{K,2}^{(i)}]$ .
7    $\mathbf{S}^{(i)} \leftarrow (\mathbf{f}^{(i)}, \mathbf{s}^{(i)}, \mathbf{p}^{(i)})$ .
8    $i \leftarrow i + 1$ .
9 end
```

F. Time Complexity and Convergence Analysis

Time complexity. We use floating point operations (flops) to analyze the time complexity. One flop is any mathematical operation (e.g., addition/subtraction/multiplication/division).

Since steps 2–8 are the bulk of Algorithm 2, we mainly analyze this part. Because Algorithm 1 is called in steps 4 and 5, we turn the view to Algorithm 1 first.

In Algorithm 1, step 3, 4 and 6 take $\mathcal{O}(K)$ flops. Step 5 takes $\mathcal{O}((i+1)K)$, where i is the smallest integer satisfying the inequality (30). Therefore, Algorithm 1's time complexity is $\mathcal{O}((i+4)K)$. Besides, in Algorithm 2, step 3 solves problem (17) through CVX. Due to the use of the interior-point algorithm in CVX, the worst time complexity is $\mathcal{O}(K^{4.5} \log \frac{1}{\epsilon})$ [28]. Note that Algorithm 2 solves SP2 by calling Algorithm 1 iteratively. Thus, the time complexity of Algorithm 2 is $\mathcal{O}(K^{4.5} \log \frac{1}{\epsilon} + 2(i+4)K)$.

Convergence Analysis. Algorithm 1 is called in Algorithm 2, so first, we discuss the convergence of Algorithm 1. The convergence proof is provided by Theorem 3.2 in [27]. Additionally, according to Theorem 3.2 in [27], Algorithm 1 converges with a linear rate at any starting point (ν^0, Γ^0) and a quadratic convergence rate of the solution's neighborhood. Therefore, Algorithm 2, which iteratively solves SP1 to get (\mathbf{f}, \mathbf{s}) and SP2_I to get \mathbf{p} , will converge eventually.

Algorithm 3: Benchmark Greedy Algorithm

```

1 Initialize  $s = s_1, C_{min} = \infty, k \in [1, K]$ 
2  $P = [p_0, \dots, p_{10}], p_i = p^{min} + 0.1i(p^{max} - p^{min})$ ,
3  $F = [f_0, \dots, f_{10}], f_i = f^{min} + 0.1i(f^{max} - f^{min})$ 
4 for  $f_{k,1}$  in  $F$  and  $f_{k,2}$  in  $F$  do
5   for  $p_{k,1}$  in  $P$  and  $p_{k,2}$  in  $P$  do
6     The energy of channel  $k$ :  $E \leftarrow \text{Eq. (3)+Eq. (4)}$ .
7     The time consumption of channel  $k$ :  $T \leftarrow \text{Eq. (2)+Eq. (6)}$ .
8      $C \leftarrow \alpha E + \beta T$ .
9     if  $C < C_{min}$  then
10      Update  $C_{min} \leftarrow C, E_{out} \leftarrow E, T_{out} \leftarrow T$ 
11    end
12  end
13 end
14 output :  $C_{min}, E_{out}, T_{out}$ 
```

IV. EXPERIMENTAL RESULTS

In this section, we evaluate experimental results: 1) the effectiveness of our proposed algorithm in the joint optimization of energy and time consumption. 2) How the global model accuracy varies with the weight parameter γ .

A. Parameter Settings

The overall system settings are provided in Table I.

Recall that the constant ξ equals $\frac{1}{s_0^2}$, and the accuracy metric $\mathcal{A}(s_{1,1}, s_{1,2}, \dots, s_{K,i})$ should be $\sum_{k=1}^K \sum_{i=1}^2 A_{k,i}(s_{k,i})$.

The optimization objective is $\alpha \mathcal{E} + \beta \mathcal{T} - \gamma \mathcal{A}$ from (9). We “normalize” the weight parameters such that $\alpha + \beta = 1$ by dividing each of them by $\alpha + \beta$. The intuition for doing this is that \mathcal{T} and \mathcal{A} are considered as “costs” and \mathcal{A} is the “gain”, then $\alpha + \beta = 1$ means the coefficient for the cost part is 1.

B. System Parameters

We have three weight parameters for the optimization problem: α , β and γ , and $\alpha + \beta = 1$. If more focus is

on energy consumption, the parameter α should be greater than β . If the delay is the objective to mainly optimize, β should be set as a larger value. Besides, the value of γ affects object detection in a similar way. To explore the influence of three parameters separately, we first implement experiments under different (α, β) with fixed γ and then show results under different γ with fixed $(\alpha, \beta) = (0.5, 0.5)$.

We compare three pairs of weight parameters $(\alpha, \beta) = (0.9, 0.1), (0.5, 0.5)$ and $(0.1, 0.9)$ with random allocation strategy and one greedy algorithm (provided in Algorithm 3). $(\alpha, \beta) = (0.9, 0.1)$ is carried out when devices are low-battery to save energy. $(\alpha, \beta) = (0.5, 0.5)$ represents the ordinary situation to equally consider time and energy. Besides, $(\alpha, \beta) = (0.1, 0.9)$ stresses the time-sensitive scenario.

Fig. 2(a), (b) and (c) show the total energy consumption \mathcal{E} , time consumption \mathcal{T} and $\alpha\mathcal{E} + \beta\mathcal{T}$ under different maximum transmission power limits. It can be observed that as the maximum transmission power increases, \mathcal{T} and $\alpha\mathcal{E} + \beta\mathcal{T}$ decrease while \mathcal{E} slightly increases. This is because as the range of p^{max} expands, there will be a more optimal solution to decrease the time consumption. Our proposed algorithm is superior to the random allocation strategy and greedy algorithm in terms of energy optimization and $\alpha\mathcal{E} + \beta\mathcal{T}$. In terms of total time consumption, the proposed algorithm performs worse than the greedy algorithm. When $(\alpha = 0.1, \beta = 0.9)$, However, it is evident that the gap is much smaller than that of energy consumption, and this is why our proposed algorithm still performs better in terms of $\alpha\mathcal{E} + \beta\mathcal{T}$.

Moreover, Fig. 3 demonstrates the performance of different algorithms under different maximum CPU frequencies. From Fig. 3(a), it can be seen the proposed algorithm performs much better than greedy algorithm in terms of energy consumption. Although the random strategy is slightly better than the green line (Proposed, $\alpha = 0.1, \beta = 0.9$) in terms of energy consumption, there is a huge gap in terms of time consumption as shown in Fig. 3(b). Still, when maximum CPU frequency increases, the gap between proposed algorithm and greedy algorithm in terms of \mathcal{E} becomes larger and larger. Although the performance of the proposed algorithm in terms of \mathcal{T}

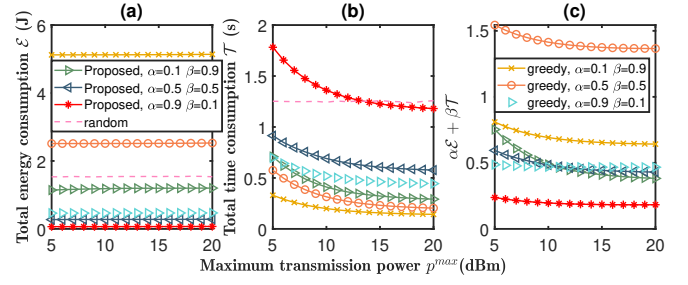


Fig. 2. Consumption under different maximum transmit power. $\gamma=1$.

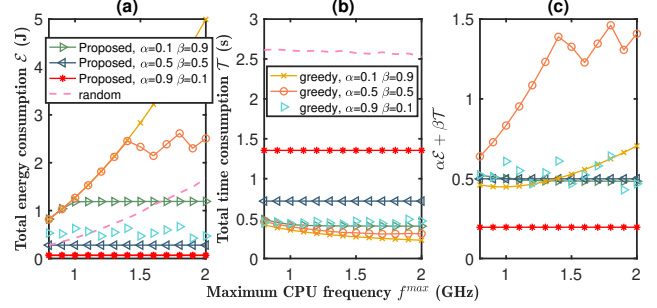


Fig. 3. Consumption under different maximum CPU frequency. $\gamma=1$.

is slightly worse than the greedy algorithm, the proposed algorithm is roughly more advantageous than the greedy algorithm in terms of $\alpha\mathcal{E} + \beta\mathcal{T}$.

C. Accuracy analysis

To analyze the selection of the frame resolution for each device under different γ and illustrate the result concisely, the number of users is set as 4. We fix the weight parameters $(\alpha, \beta) = (0.5, 0.5)$ and choose different γ , to calculate corresponding optimal video resolution for each user as shown in Fig. 4(a) and illustrate the relationship between γ and model accuracy in Fig. 4(b). YOLOv5m [29], which is one of the object detection architectures You Only Look Once (YOLO), is implemented for each user under federated learning setting. The dataset is COCO [30]. This experiment environment is on a workstation with three NVIDIA RTX 2080 Ti GPUs for computation acceleration.

There are 4 lines in Fig. 4(a) which represent the resolution choices for 4 users. Obviously, as γ increases, which means the system will pay more attention on model accuracy, users are more inclined to choose higher video resolution. Because such selections of s could bring prominent improvement for model accuracy, which could be noticed in Fig. 4(b). When γ is lower than around 0.85, 4 users will always choose the lowest resolution $s_1 = 160$ and the model accuracy is only about 0.32. After γ reach 0.85, users begin to pick resolution $s_2 = 320$ and the model accuracy increase to about 0.40. Besides, if γ gets bigger, users will adopt the highest available resolution $s_3 = 640$ and so there is a dramatically improvement in accuracy, reaching approximately 0.68.

V. CONCLUSION

In this work, an FL-assisted MAR system via NOMA is proposed. We have explored the problem of joint optimiza-

TABLE I
SYSTEM PARAMETER SETTING

Parameter	Value
The path loss model	$128.1 + 37.6 \log(d \text{ (km)})$
The standard deviation of shadow fading	8 dB
Noise power spectral density N_k	-174 dBm/Hz
The number of users N	50
The number of channels K	25
Total Bandwidth (B)	20 MHz
CPU frequency f^{max}, f^{min}	2 GHz, 0 GHz
The number of CPU cycles c_n	Randomly assigned in $[1, 3] \times 10^4$
Transmission power p^{max}, p^{min}	12 dBm, 0 dBm
The number of local iterations η	10
The data size uploaded d_n	28.1 kbits
The number of samples D_n	500
Effective switched capacitance $kappa$	10^{28}
Video frame resolutions (s_0, s_1, s_2, s_3)	(100, 160, 320, 640) pixels

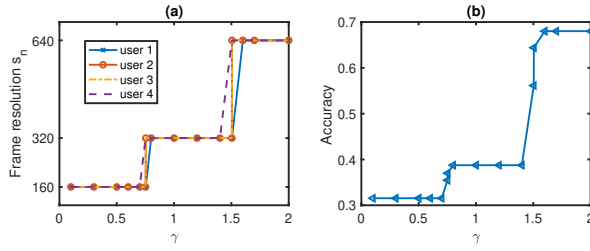


Fig. 4. Frame resolution and accuracy under different γ . Here $(\alpha, \beta) = (0.5, 0.5)$.

tion of energy, time and accuracy to allocate appropriate transmission power, computational frequency and video frame resolution for each device in the system. Through adjusting three weight parameters in the optimization problem, our proposed algorithm can be adapted to various scenarios. Time complexity and convergence analysis are also provided for the proposed resource allocation algorithm. In experimental results, it can be observed that our proposed algorithm is particularly effective in optimizing energy consumption compared to random allocation strategy and a benchmark greedy algorithm. Our paper also provides new insights into how federated learning and MAR can be applied to the Metaverse.

ACKNOWLEDGEMENT

This research is partly supported by the Singapore Ministry of Education Academic Research Fund under Grant Tier 1 RG90/22, RG97/20, Grant Tier 1 RG24/20 and Grant Tier 2 MOE2019-T2-1-176; and partly by the NTU-Wallenberg AI, Autonomous Systems and Software Program (WASP) Joint Project.

REFERENCES

- [1] J. D. N. Dionisio, W. G. B. III, and R. Gilbert, "3D virtual worlds and the metaverse: Current status and future possibilities," *ACM Computing Surveys (CSUR)*, vol. 45, no. 3, pp. 1–38, 2013.
- [2] B. McMahan, E. Moore, D. Ramage, S. Hampson, and B. A. y Arcas, "Communication-efficient learning of deep networks from decentralized data," in *Artificial intelligence and statistics*. PMLR, 2017, pp. 1273–1282.
- [3] Q. C. Li, H. Niu, A. T. Papathanassiou, and G. Wu, "5G network capacity: Key elements and technologies," *IEEE Vehicular Technology Magazine*, vol. 9, no. 1, pp. 71–78, 2014.
- [4] Y. Chen, B. Wang, Y. Han, H.-Q. Lai, Z. Safar, and K. R. Liu, "Why time reversal for future 5G wireless?[perspectives]," *IEEE Signal Processing Magazine*, vol. 33, no. 2, pp. 17–26, 2016.
- [5] C. He, H. Wang, Y. Hu, Y. Chen, X. Fan, H. Li, and B. Zeng, "Mcast: High-quality linear video transmission with time and frequency diversities," *IEEE Transactions on Image Processing*, vol. 27, no. 7, pp. 3599–3610, 2018.
- [6] A. Benjebbour, Y. Saito, Y. Kishiyama, A. Li, A. Harada, and T. Nakamura, "Concept and practical considerations of non-orthogonal multiple access (noma) for future radio access," in *2013 International Symposium on Intelligent Signal Processing and Communication Systems*. IEEE, 2013, pp. 770–774.
- [7] T. Song, X. Tan, J. Ren, W. Hu, S. Wang, S. Xu, X. Wang, G. Sun, and H. Yu, "Dram: A drl-based resource allocation scheme for mar in mec," *Digital Communications and Networks*, 2022. [Online]. Available: <https://www.sciencedirect.com/science/article/pii/S2352864822000633>
- [8] A. Al-Shuwaili and O. Simeone, "Energy-efficient resource allocation for mobile edge computing-based augmented reality applications," *IEEE Wireless Communications Letters*, vol. 6, no. 3, pp. 398–401, 2017.
- [9] X. Chen and G. Liu, "Energy-efficient task offloading and resource allocation via deep reinforcement learning for augmented reality in mobile edge networks," *IEEE Internet of Things Journal*, vol. 8, no. 13, pp. 10 843–10 856, 2021.

- [10] X. Chen and G. Liu, "Joint optimization of task offloading and resource allocation via deep reinforcement learning for augmented reality in mobile edge network," in *2020 IEEE International Conference on Edge Computing (EDGE)*. IEEE, 2020, pp. 76–82.
- [11] P. Si, J. Zhao, H. Han, K.-Y. Lam, and Y. Liu, "Resource allocation and resolution control in the metaverse with mobile augmented reality," *arXiv preprint arXiv:2209.13871*, 2022.
- [12] M. Makolkina, A. Paramonov, and A. Koucheryavy, "Resource allocation for the provision of augmented reality service," in *Internet of Things, Smart Spaces, and Next Generation Networks and Systems*, O. Galinina, S. Andreev, S. Balandin, and Y. Koucheryavy, Eds. Cham: Springer International Publishing, 2018, pp. 441–455.
- [13] J. Li, F. Wu, K. Zhang, and S. Leng, "Joint dynamic user pairing, computation offloading and power control for noma-based mec system," in *2019 11th International Conference on Wireless Communications and Signal Processing (WCSP)*. IEEE, 2019, pp. 1–6.
- [14] Y. Ye, R. Q. Hu, G. Lu, and L. Shi, "Enhance latency-constrained computation in mec networks using uplink noma," *IEEE Transactions on Communications*, vol. 68, no. 4, pp. 2409–2425, 2020.
- [15] S. Gupta, D. Rajan, and J. Camp, "Noma-enabled computation and communication resource trading for a multi-user mec system," *IEEE Transactions on Vehicular Technology*, 2022.
- [16] D. Chen, L. J. Xie, B. Kim, L. Wang, C. S. Hong, L.-C. Wang, and Z. Han, "Federated learning based mobile edge computing for augmented reality applications," in *IEEE ICNC*. 2020, pp. 767–773.
- [17] Z. Zhang, H. Sun, and R. Q. Hu, "Downlink and uplink non-orthogonal multiple access in a dense wireless network," *IEEE Journal on Selected Areas in Communications*, vol. 35, no. 12, pp. 2771–2784, 2017.
- [18] C. He, Y. Hu, Y. Chen, and B. Zeng, "Joint power allocation and channel assignment for noma with deep reinforcement learning," *IEEE Journal on Selected Areas in Communications*, vol. 37, no. 10, pp. 2200–2210, 2019.
- [19] C. T. Dinh, N. H. Tran, M. N. Nguyen, C. S. Hong, W. Bao, A. Y. Zomaya, and V. Gramoli, "Federated learning over wireless networks: Convergence analysis and resource allocation," *IEEE/ACM Trans. on Networking*, vol. 29, no. 1, pp. 398–409, 2021.
- [20] Z. Yang, M. Chen, W. Saad, C. S. Hong, and M. Shikh-Bahaei, "Energy efficient federated learning over wireless communication networks," *IEEE Trans. on Wireless Comm.*, vol. 20, no. 3, pp. 1935–1949, 2021.
- [21] J. Redmon, S. Divvala, R. Girshick, and A. Farhadi, "You Only Look Once: Unified, Real-Time Object Detection," in *Proceedings of the IEEE Conference on Computer Vision and Pattern Recognition*, 2016, pp. 779–788.
- [22] A. Krizhevsky, I. Sutskever, and G. E. Hinton, "Imagenet Classification with Deep Convolutional Neural Networks," *Advances in Neural Information Processing Systems*, vol. 25, 2012.
- [23] Y. Mao, J. Zhang, and K. B. Letaief, "Dynamic Computation Offloading for Mobile-Edge Computing with Energy Harvesting Devices," *IEEE Journal on Selected Areas in Communications*, vol. 34, no. 12, pp. 3590–3605, 2016.
- [24] Q. Liu, S. Huang, J. Opadere, and T. Han, "An Edge Network Orchestrator for Mobile Augmented Reality," in *IEEE Conference on Computer Communications (INFOCOM)*. IEEE, 2018, pp. 756–764.
- [25] M. Grant and S. Boyd, "CVX: Matlab software for disciplined convex programming, version 2.1," 2014.
- [26] R. W. Freund and F. Jarre, "Solving the sum-of-ratios problem by an interior-point method," *Journal of Global Optimization*, vol. 19, no. 1, pp. 83–102, 2001.
- [27] Y. Jong, "An Efficient Global Optimization Algorithm for Nonlinear Sum-of-Ratios Problem," *Optimization Online*, 2012.
- [28] Z.-Q. Luo, W.-K. Ma, A. M.-C. So, Y. Ye, and S. Zhang, "Semidefinite Relaxation of Quadratic Optimization Problems," *IEEE Signal Processing Magazine*, vol. 27, no. 3, pp. 20–34, 2010.
- [29] G. Jocher, A. Chaurasia, A. Stoken, J. Borovec, NanoCode012, Y. Kwon, TaoXie, K. Michael, J. Fang, imyhxy, Lorna, C. Wong, Z. Yifu, A. V. D. Montes, Z. Wang, C. Fati, J. Nadar, Laughing, UnglvKitDe, tkianai, yxNONG, P. Skalski, A. Hogan, M. Strobel, M. Jain, L. Mammana, and xlyieong, "ultralytics/yolov5: v6.2 - YOLOv5 Classification Models, Apple M1, Reproducibility, ClearML and Deci.ai integrations," Aug. 2022. [Online]. Available: <https://doi.org/10.5281/zenodo.7002879>
- [30] T.-Y. Lin, M. Maire, S. Belongie, J. Hays, P. Perona, D. Ramanan, P. Dollár, and C. L. Zitnick, "Microsoft coco: Common objects in context," in *European conference on computer vision*. Springer, 2014, pp. 740–755.